Supporting Information

Simultaneous enhancement of power factor and suppression of thermal conductivity in bulk $TlFe_{1.6}Se_2$ via embedded atomically thin FeSe layers

Xinyi He[1,2,§], *Katsuma Ogata*[1,§], *Terumasa Tadano*[3], *Hidenori Hiramatsu*[1,4], *Toshio Kamiya*[1,4], *and Takayoshi Katase*[1,*]

[1] Materials and Structures Laboratory, Institute of Integrated Research, Institute of Science Tokyo, 4259 Nagatsuta, Midori, Yokohama, 226-8501, Japan

[2] Kanagawa Institute of Industrial Science and Technology, 705-1 Shimoimaizumi, Ebina, Kanagawa 243-0435, Japan

[3] Research Center for Magnetic and Spintronic Materials, National Institute for Materials Science, 1-2-1 Sengen, Tsukuba, Ibaraki 305-0047, Japan

[4] MDX Research Center for Element Strategy, Institute of Integrated Research, Institute of Science Tokyo, 4259 Nagatsuta, Midori, Yokohama 226-8501, Japan

* Correspondence to: katase.t.aa@m.titech.ac.jp

Contents

Crystal structure and microstructures

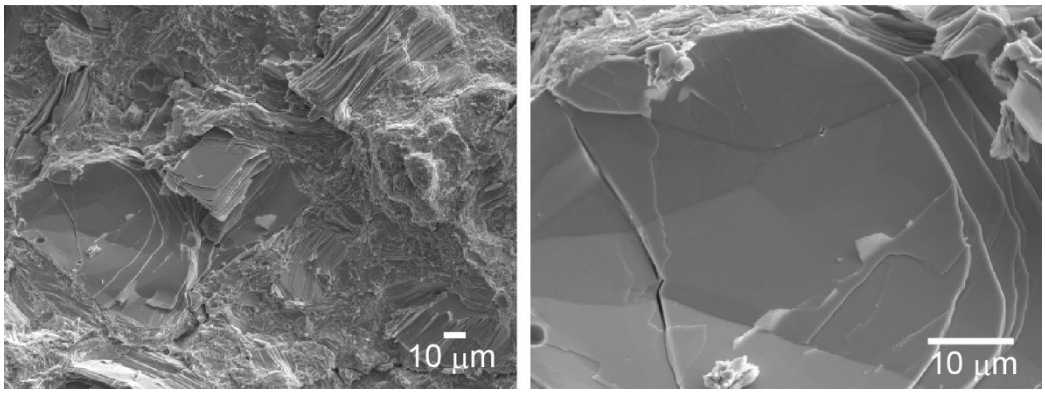

Figure S1. Microstructure of the broken-out surface of $TlFe_{1.6}Se_2$ bulk polycrystal observed by EPMA. The average chemical composition based on 10-point EPMA analysis was Tl : Fe : Se = 1 : 1.67 : 1.97.

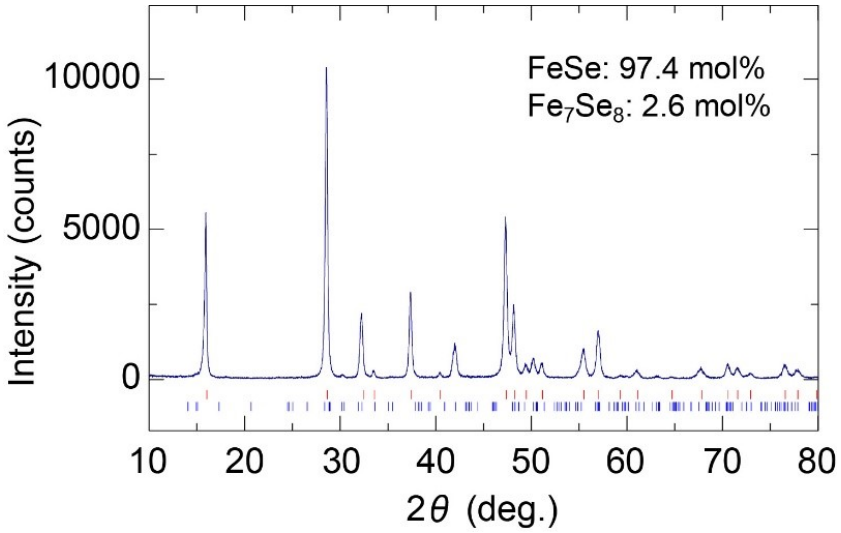

Figure S2. (a) XRD pattern of FeSe bulk sample at RT. The main diffraction peaks were assigned to α-FeSe phase (space group: $P4/nmm$), while a small amount of impurity phase of Fe_7Se_8 ($P3_121$) were detected.

Thermal transport properties

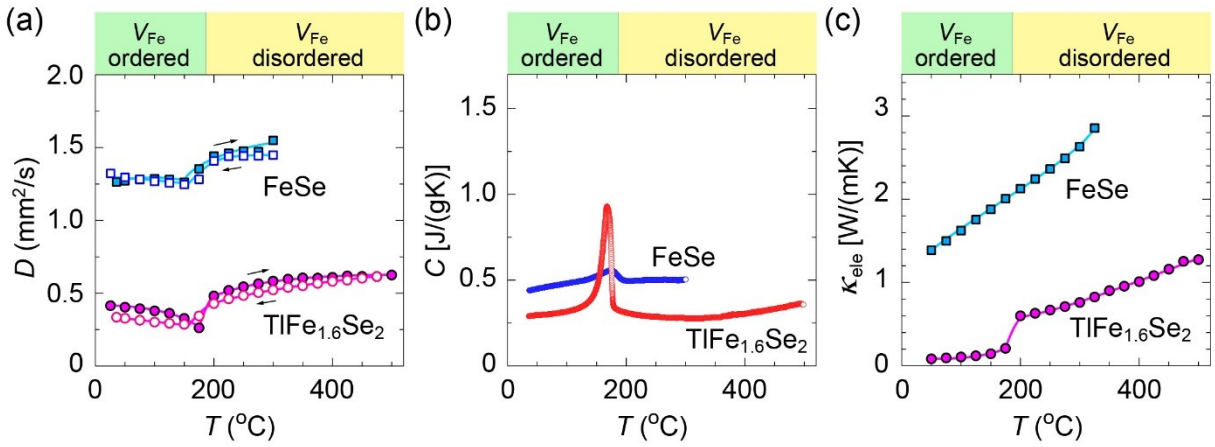

Figure S3. T dependence of (a) thermal diffusivity (D), (b) heat capacity (C), and (c) electronic thermal conductivity (κ_{ele}) for bulk samples of $TlFe_{1.6}Se_2$ and FeSe.

Thermoelectric property analysis

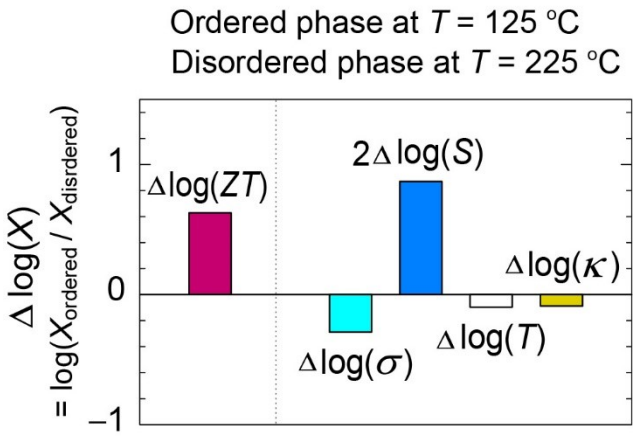

Figure S4. Decomposition of the contributions in the ZT change across the V_{Fe} order–disorder transition, evaluated between the V_{Fe}-ordered phase at 125 °C and the V_{Fe}-disordered phase at 225 °C. Here, $\Delta\log(X) = \log(X_{ordered}/X_{disordered})$; positive (negative) values indicate parameters that enhance (reduce) ZT in the V_{Fe}-ordered phase.

Calculations

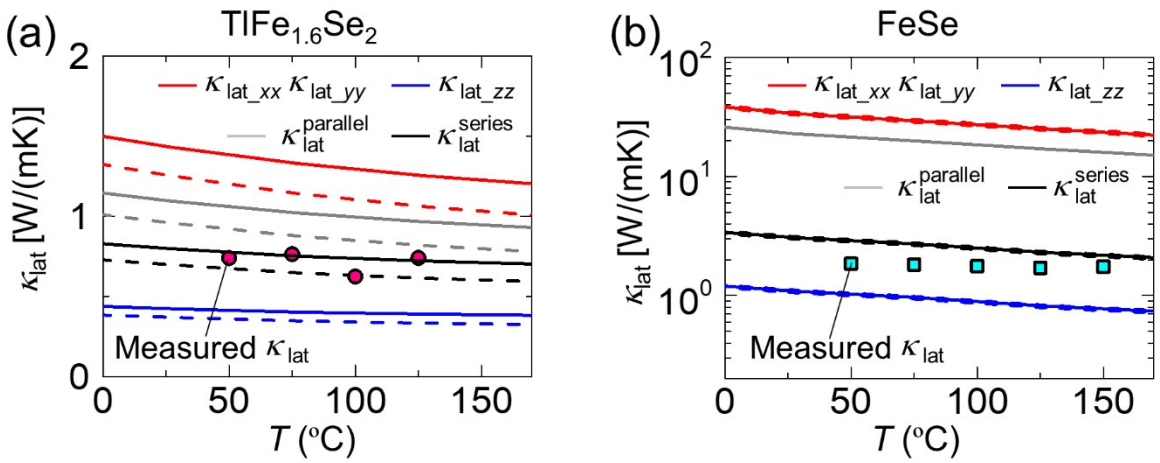

Figure S5. Temperature dependence of the calculated κ_{lat} along *xx*- and *yy*-axes (parallel to FeSe layer) and the *zz*-axis (perpendicular to FeSe layer) for (a) $TlFe_{1.6}Se_2$ and (b) FeSe with (solid lines) and without (dashed lines) the contribution from the coherent term. The averaged κ_{lat} values obtained using the series conduction model ($\kappa_{lat}^{series} = (\frac{1}{\kappa_{xx}} + \frac{1}{\kappa_{yy}} + \frac{1}{\kappa_{zz}})^{-1} \times 3$) and the parallel conduction model ($\kappa_{lat}^{parallel} = \frac{\kappa_{xx} + \kappa_{yy} + \kappa_{zz}}{3}$) are also shown. The experimentally measured κ_{lat} for V_{Fe}-ordered $TlFe_{1.6}Se_2$ and FeSe polycrystals are plotted for comparison.

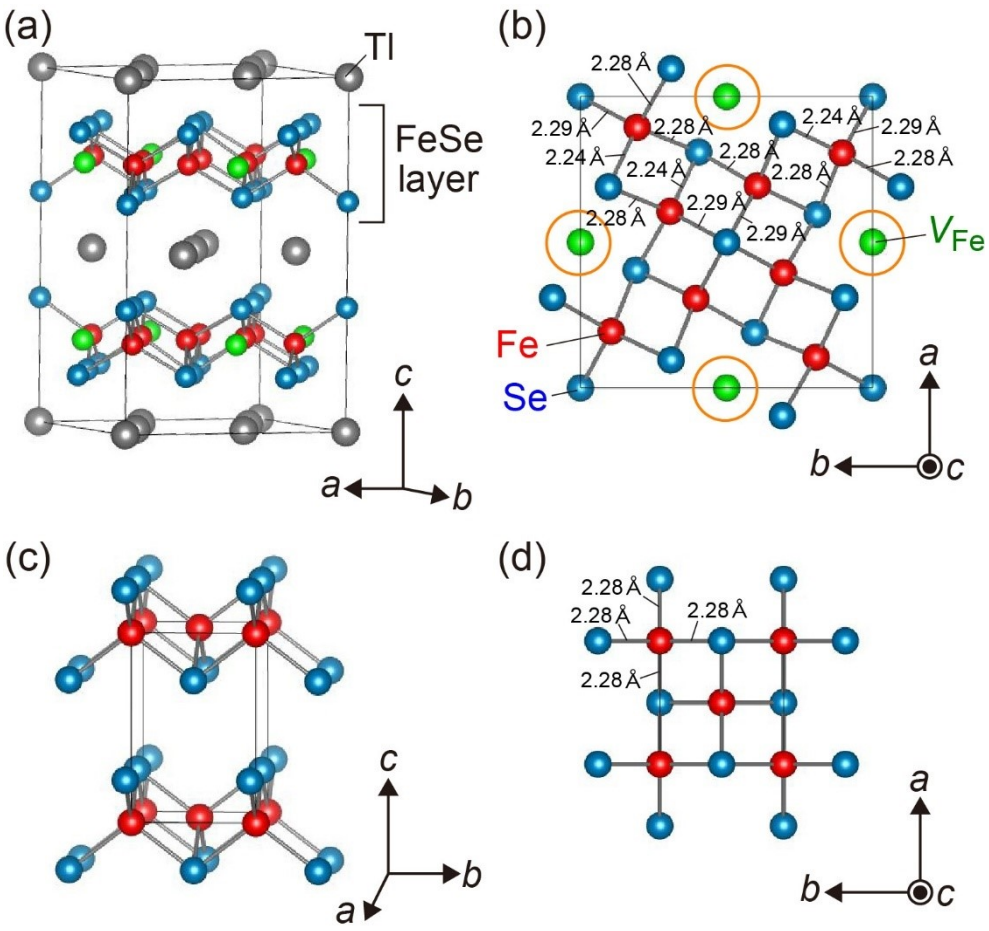

Figure S6. Fully relaxed crystal structures of (a,b) $TlFe_{1.6}Se_2$ and (c,d) FeSe models. Tl, Fe, Se atoms are depicted by gray, red, and blue spheres, respectively, and Fe-vacancy (V_{Fe}) sites are indicated by green spheres. The calculated lattice parameters of $TlFe_{1.6}Se_2$ are $a = b = 8.49$ Å, and $c = 12.78$ Å, respectively. Those of FeSe are $a = b = 3.615$ Å and $c = 5.52$ Å. In (b), Fe–Se bond lengths in $TlFe_{1.6}Se_2$ are highlighted, illustrating the local bond-length variation around V_{Fe} sites. In (d), the Fe–Se bond lengths in FeSe are shown for comparison.

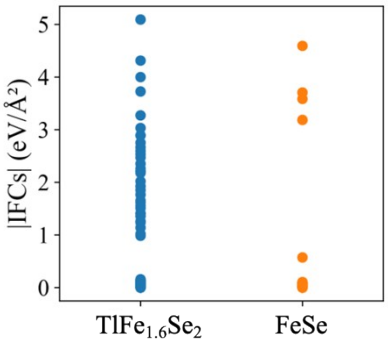

Figure S7. Comparison of the second-order interatomic force constants (IFCs) of Fe-Se interactions for $TlFe_{1.6}Se_2$ and FeSe.

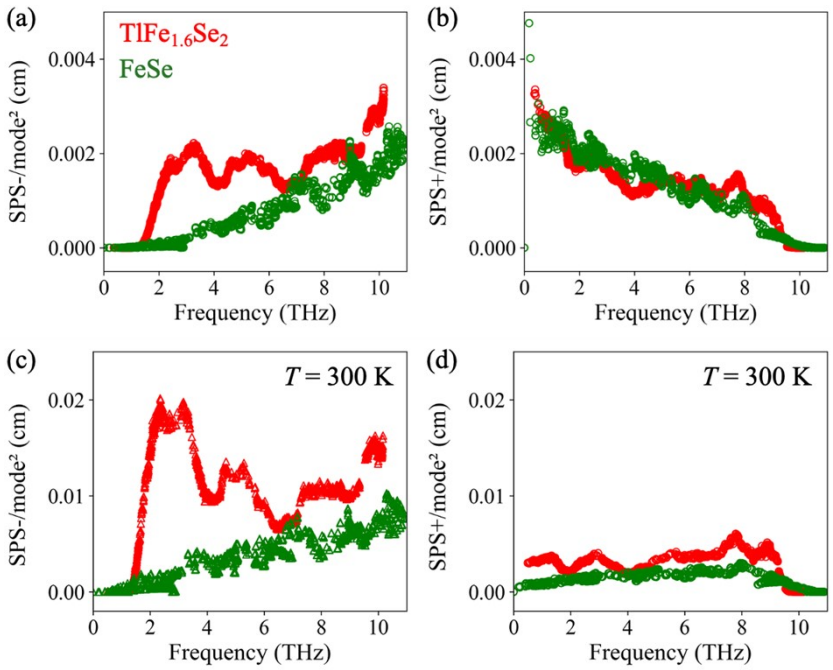

Figure S8. Three-phonon scattering phase space (SPS). (a, b) SPS without occupation factors and (c, d) SPS with occupation factors at $T = 300$ K. The left panels correspond to emission (−) processes and the right panels correspond to absorption (+) processes. Red markers represent $TlFe_{1.6}Se_2$ and green markers represent FeSe. To ensure a consistent comparison between different supercells, the SPS is normalized by the square of the number of phonon modes ($mode^2$). Compared to FeSe, the defective structure $TlFe_{1.6}Se_2$ shows a clear enhancement of the emission (−) SPS across the frequency range, particularly in the 1.5–4 THz region, consistent with the reduced phonon lifetimes in this frequency range (**Figure 6b**).